RSC Advances

ROYAL SOCIETY OF CHEMISTRY

www.rsc.org/advances

Structure of fully asymmetric mixed electrolytes around a charged nanoparticle: A density functional and simulation investigation

Chandra N. Patra*

Theoretical Chemistry Section, Chemistry Group,

Bhabha Atomic Research Centre, Mumbai 400 085, India

Abstract

A systematic study on the structure of mixed electrolytes with arbitrary size and charge asymmetry around a charged nanoparticle is carried out using density functional theory and Monte Carlo simulation. A primitive model representation with the spherical macroion surrounded by small ions in a continuum dielectric as the solvent, is used. A weighted density approximation is used to evaluate the hard-sphere correlation, whereas the ionic part is calculated using perturbation expansion around the bulk density. A canonical ensemble Monte Carlo simulation on the same system is also performed, for comparison. Parametric variations on component ratios of the electrolyte, ionic concentrations, surface charge densities and macroion as well as small ions sizes show interesting phenomena of overcharging and charge reversals. The theoretical predictions are found to be in good agreement with the simulation results concerning the density as well as mean electrostatic potential profiles. The present study shows distinctive evidence of size and charge correlations around the interface, in a fully asymmetric situation.

I. INTRODUCTION

Modern technological developments of any process, instrument or design depends on the very nature of interacting forces between its components and the communications amongst each other.[1] This not only allows tunability but also throws a deeper understanding of intermolecular interactions leading to newer methodologies of fabrication.[2] A substantial part of intermolecular interactions involves that of charged systems, that is extremely important in determining the stability and dynamical information of self-assembly, common synthetic processes for nanomaterials.[3] The layer-by-layer assembly and its suitability for different systems solely depend on the size, shape as well symmetry of the materials involved.[4] In essence, the nano-electromechanical devices, commonly used for drug delivery[5] and multiscale electronics is also fabricated from the through knowledge of the intermolecular potentials at the interface apart from that in the bulk.[6]

Macromolecular solutions denote another class of substances where interfacial interactions play a vital role and quality and quantity of the same has been used to predict a number of interfacial phenomena encompassing electrochemistry, biology, materials science, etc.[7] The interfacial interactions also provides detailed understanding of nurturing of properties of technologically important polyelectrolytes used in agricultural engineering and food science, paints, varnishes, etc.[8] This particular subject has found utmost attention over the last decade due to the feasibility of measurements of subtle length and time scales.[9] Thus optical tweezer measurements[10] in colloidal solutions provide direct evidence of attraction in likely charged systems. Similarly, confocal microscopy[11] in bilayers and biological systems give direct imaging of the topology of layers and their interactions.

The colloidal solution alongwith supporting electrolytes leads to the formation of electric double layers (EDL),[12,13] where the first layer (so-called Helmholtz layer) remain within the size of the counterion and the diffuse layer extends beyond that depending on the electrostatic interactions between the component ions and also with the interface. The geometry of the system merely determines the geometry of the respective double layer, i.e., spherical double layer (SDL) for the case of colloidal solution.[14] However, when the colloidal macroion becomes sufficiently large, the symmetry of the system tends to a planar one, resulting into planar double layers.[15] Similarly, the biomacromolecular solutions as well as DNA represents the cylindrical double layers.[16] EDLs are subjected to rigorous theoretical studies mainly

because of a wide variety of parametric variations leading to different types of double layers. Most of these studies are restricted to model systems as the applicability of the theoretical calculations can be compared to that of computer simulations. These studies also forward proper understanding about the suitability or refinement of different models used in double layer theories.

The theoretical studies on EDLs started with the point-ion Poisson-Boltzmann (PB) description,[17] however, the introduction of correlations has emerged only in the last decades, thereby, modified Poisson-Boltzmann theory,[18] integral equation theory (IET),[19] density functional theory (DFT)[20] and their different variants have taken their course in the last few years to study the EDL in detail. All these studies not only improved the fundamental understanding but also proposed suitable applications of the same into even more complex systems. Planar[21–26] and cylindrical[27–30] EDLs have been studied extensively because of their applicability to electrochemical cells, synthetic polyelectrolytes, and DNA, however, the SDLs has attracted a great deal of attention with the advent of mechanisms of fabrication of nanomaterials through suitable modifications and assembling of spherical nanoparticles. In most of these studies, restricted primitive model (RPM)[12] is used, where the electrode is a structureless large hard sphere with uniform surface charge density and small ions as charged hard spheres with equal diameter embedded in a solvent of dielectric continuum. This model is extended to include solvent as a component as solvent primitive model (SPM).[31] Efforts to include different sized small ions beyond the RPM has been worked out in great detail recently,[32–36] although the PB solution for the system has been known over the years.[37] Thus, IET involving hypernetted chain/mean spherical approximation (HNC/MSA) and Monte Carlo (MC) simulations has been used quite extensively by Guerrero-García *et al*[34,36,38–40] to study the effect of size and charge asymmetry on SDL. The other contributions require mention here are reference hypernetted chain approximations,[32] reference fluid density functional approaches,[33] and and the exclusion volume corrected PB theory.[35] The important inferences that counterions do not always determine the properties of the double layers and the presence of potential of zero charge in size-asymmetric SDL as compared to its presence in certain cases in size-symmetric one has been revealed in all these works.

Due to its ensuing success in handling classical correlations, DFT has been applied to size-asymmetric SDL in recent times. Thus, Kim *et al*[41] applied a perturbative DFT, with

hard-sphere component of the excess free energy from the Percus-Yevick equation and ionic part through a perturbation expansion around the uniform fluid. Another perturbative DFT involving approximating hard sphere part through fundamental measure theory is also applied[42] on the same system in RPM, SPM, as well as solvent RPM. In both the cases, the theoretical results seem to reproduce the MC data quite well. In a recent work,[43] we carried out a comprehensive study using DFT and MC simulations on a fully asymmetric SDL, i.e., with both charge and size asymmetry of its components. The theoretical predictions compare quite quantitatively with that of simulations results and provide interesting observations of overcharging (OC)[44] and charge reversal (CR)[28] phenomena.

Mixed salts containing ionic components having different valance and sizes are quite important[45] in many macromolecular and biological phenomena[46] and hence been the subject of present day research.[42] The structure of SDL containing mixed electrolytes within RPM has been studied in detail[47] and important observations of CR with the gradual addition of multivalent ions has been reported.[48] Planar[49,50] as well as cylindrical EDL[51] system containing mixed electrolytes within the RPM has also been studied. Since it is now quite well known that the presence of multivalent ions have a major influence in size-asymmetric SDL, it would be worthwhile to work on such basic electrolyte system containing arbitrary charge and size asymmetry. The theoretical formalism and the MC simulation method remains to be the same as reported in binary electrolyte case.[43] Thus, the partially perturbative DFT used here considers weighted density approach (WDA) for the hard-sphere part and the perturbation around the uniform fluid for the residual ionic component. The presence of multivalent ions on the charge and size asymmetric electrolyte is studied in terms of density as well as mean electrostatic potential profiles of the SDL under different parametric conditions, viz. concentration of the multivalent ions, bulk concentration of electrolyte, surface charge density, size of the macroion, and the size of the small ions. In section II, we present the model and formalisms, the results and discussion part is presented in Section III and the concluding remarks in Section IV.

II. THEORETICAL FORMULATION

A. Model for the system

The system we consider here is a primitive model (PM) mixed electrolyte near a hard charged spherical nanoparticle. The solvent is implicitly included in the system using a continuum dielectric constant as that of water, $\epsilon = 78.5$ at temperature, $T = 298$ K. The small ions (α) are modeled as charged hard spheres of diameter σ_α, so that the pair potential is given as

$$u_{\alpha\beta}(r) = \begin{cases} \infty, & r < \frac{\sigma_\alpha+\sigma_\beta}{2}, \\ \frac{z_\alpha z_\beta e^2}{\epsilon r}, & r > \frac{\sigma_\alpha+\sigma_\beta}{2} \end{cases} . \tag{1}$$

with z_α as the valence and e is the electronic charge. The macroion is of radius R with a total charge $Z_M e$ concentrated at its center resulting into uniform surface charge density Q as

$$Q = \frac{Z_M e}{4\pi R^2} \quad . \tag{2}$$

Therefore, the macroion-ion interaction potential is written as

$$U_{M\alpha}(r) = \begin{cases} \infty, & r < R + \frac{\sigma_\alpha}{2}, \\ \frac{4\pi R^2 Q z_\alpha e}{\epsilon r}, & r > R + \frac{\sigma_\alpha}{2}, \end{cases} \tag{3}$$

Although the above equations are written in CGS form, SI units are actually used for different parameters as mentioned throughout the text. In the present work, the diameter ratios for the ions in the mixed electrolyte is always taken as 1:2:3 as $\sigma_1 = \sigma,\ \sigma_2 = 2\sigma,\ \sigma_3 = 3\sigma$, with the smallest ionic diameter (σ) as 0.2125 nm. The multivalent ion is always taken as the smallest one that follows from the analysis of Rakitin and Pack,[52] about the use of bare ionic diameters without hydration shell. It should be worth noting that the diameter ratios chosen here are only representative one and the theoretical formalism is equally applicable for any arbitrary diameter ratios. Also because of the presence of three different sized small ions in the PM electrolyte, there appears three Helmholtz planes, viz. the inner Helmholtz plane (IHP) and two outer Helmholtz planes (OHP) at distances $R + \sigma_\alpha/2,\ \alpha = 1, 2, 3$, respectively, as compared to only single Helmholtz plane at $R + \sigma/2$ for size-symmetric ($\sigma_1 = \sigma_2 = \sigma_3 = \sigma$) SDL.

B. Density Functional Theory

The central part of a DFT is to express the grand potential Ω or the free energy F of the system as a functional of singlet density distributions $\{\rho_\alpha(\mathbf{r})\}$. For the present system of SDL, the two are connected through a Legendre transform, viz.,

$$\Omega[\{\rho_\alpha\}] = F[\{\rho_\alpha\}] + \sum_\alpha \int d\mathbf{r}\rho_\alpha(\mathbf{r})[U_{M\alpha}(\mathbf{r}) - \mu_\alpha], \tag{4}$$

where μ_α is the chemical potential due to the component ion α. At equilibrium, the grand potential attains a minimum value with respect to variation in the density distribution and this condition is regularly used to calculate the density profiles as well as the grand free energy. The major work in DFT still remains to find a better expression for free energy or the equation of state and the suitability of different approximations in this method lead to various versions of DFT. Without going into details, the final expression for the density profiles goes as

$$\begin{aligned}\rho_\alpha(r) \;=\; \rho_\alpha^0 \exp\big\{&-\beta_0 z_\alpha \psi(r) + c_\alpha^{(1)\,hs}(r;[\{\rho_\alpha\}]) - c_\alpha^{(1)\,hs}([\{\rho_\alpha^0\}]) \\ &+ c_\alpha^{(1)\,el}(r;[\{\rho_\alpha\}]) - c_\alpha^{(1)\,el}([\{\rho_\alpha^0\}])\big\}\,,\end{aligned} \tag{5}$$

where $\beta_0 = (k_B T)^{-1}$, with k_B as the Boltzmann constant and T as the temperature and $c_\alpha^{(1)}(\mathbf{r};[\{\rho_\alpha]])$ represents the first-order correlation function. In Eq. (5), $\psi(\mathbf{r})$ is the mean electrostatic potential of the diffused layer arises due to macroion surface charge and the small ion distributions and can be expressed as[53]

$$\psi(r) = \frac{4\pi e}{\epsilon}\int_r^\infty \sum_\alpha z_\alpha \rho_\alpha(r')\left(r' - \frac{r'^2}{r}\right)dr' \quad . \tag{6}$$

Although Eq. (5) for the density profile is formally exact, it still requires approximations for $c_\alpha^{(1)\mathrm{hs}}$ and $c_\alpha^{(1)\mathrm{el}}$ for the nonuniform SDL system. In a recent work, we adopted a partially perturbative approach to calculate these two quantities for a SDL with arbitrary size and charge asymmetry. In this approach, the quantity, $c_\alpha^{(1)\,hs}(x;[\{\rho_\alpha\}])$ is calculated using the weighted density approximation of Denton and Ashcroft (DA)[54] as

$$c_\alpha^{(1)\mathrm{hs}}(\mathbf{r};[\{\rho_\alpha\}]) = \tilde{c}_\alpha^{(1)\mathrm{hs}}(\bar{\rho}^{(\alpha)}(\mathbf{r})) \quad , \tag{7}$$

where, $\tilde{}$ represents its uniform fluid counterpart and the weighted density, $\bar{\rho}_\alpha(\mathbf{r})$ is calculated using DA prescription. The electrical contribution, $c_\alpha^{(1)el}(\mathbf{r};[\{\rho_\alpha\}])$is obtained by a

perturbative expansion around a uniform fluid as

$$c_{\alpha}^{(1)el}(\mathbf{r};[\{\rho_{\alpha}\}]) = \tilde{c}_{\alpha}^{(1)el}([\{\rho_{\alpha}^{0}\}]) + \sum_{\beta}\int d\mathbf{r}'\tilde{c}_{\alpha\beta}^{(2)el}(|\mathbf{r}-\mathbf{r}'|;[\{\rho_{\alpha}^{0}\}])\left(\rho_{\beta}(\mathbf{r}')-\rho_{\beta}^{0}\right) \quad . \tag{8}$$

The direct correlation functions, $\tilde{c}_{\alpha\beta}^{(2)hs}$ and $\tilde{c}_{\alpha\beta}^{(2)el}$ for the PM electrolyte are taken from the analytical expressions within the mean spherical approximation as given by Blum[55] and Hiroike[56] for arbitrary ionic size and charge asymmetry. Once the approximate first order correlations functions are obtained through Eqs. (7) and (8), the density and the mean electrostatic potential profiles are calculated from Eqs. (5) and (6) using a Picard iteration. The convergence criterion is chosen in such a way that after nth iteration, the norm defined as $\left[\sum\alpha\sum_{i=1}^{N}\left(\left\{\rho_{\alpha}^{(n)}(r_i)-\rho_{\alpha}^{(n-1)}(r_i)\right\}/\rho_{\alpha}^{0}\right)^{2}/2N\right]^{1/2}$ attains a small value ($< 10^{-6}$), where N is the total number of mesh points.

C. Monte Carlo Simulations

In the present work, we adopt a canonical Monte Carlo (CMC) simulations (N,V,T) using standard Metropolis sampling procedure.[57] A cubic simulation box with the macroion fixed at the center is populated with the mixed electrolyte system until the desired concentration is achieved. The simulation cell so chosen is sufficiently large to avoid interactions between the macroions. The entire system remains electroneutral, $\sum_{\alpha}N_{\alpha}z_{\alpha}+Z_{M}e=0$, with N_{α} as the number of ions. The periodic boundary conditions are employed in all directions. The long-range Coulomb interactions are treated with the Ewald sum method under conducting boundary conditions.[58] Because of spherical geometry, the ions are translated in a random direction at a random amount and change in potential energy (ΔU) is calculated for the acceptance criteria. The acceptance ratio for total moves is kept below 0.5. The block averaging procedure is used for final averaging over 10 blocks each having 10^{7} moves.

III. RESULTS AND DISCUSSION

The present work is aimed at a systematic study of the structure of size-asymmetric SDL consisting of a spherical macroion surrounded by the PM electrolyte containing the mixture of mono and multivalent ions. In order to visualize the effect of multivalent ions, 1:1 (NaCl) electrolyte is mixed by gradual addition of 2:1 ($MgCl_2$) to have a mixed salt

representation, 1:2:1 ($NaCl/MgCl_2$). The ionic density profiles of such a SDL system of 1M NaCl with varying concentrations of $MgCl_2$ around a spherical macroion of $R = 1.5$ nm with $Q = 0.102$ Cm^{-2} ($Z_M = 18$) is presented in Fig. 1. As is obvious, there is a considerable accumulation of Cl^- and depletion of both Na^+ and Mg^{2+} at the macroparticle surface, purely due to the energetic preference in terms of attraction of counterions and repulsion of coions. The addition of small amount of smallest divalent coions [Mg^{2+}] does not change the Cl^- density profile substantially in contrary to the size-symmetric case.[48] However, there is a gradual increase in the Na^+ and Mg^{2+} densities at the interface like that of the size-symmetric electrolytes.[48] Presence of coions at the surface leads to considerable OC effect. This definitely corroborates the fact[34] that counterions do not determine the double layer properties in the size-asymmetric electrolytes. As the concentration of Mg^{2+} increases, there is increased screening of macroion charge by Cl^- as well as Na^+ and Mg^{2+}, leading to increased CR. Increased electrostatic interaction between the macroion and the small ions also leads to damping of the density profiles as one goes on increasing the divalent coions (Mg^{2+}).

The increased charge inversion is also reflected in the mean electrostatic potential (MEP) profiles for systems of varying [Mg^{2+}]:[Na^+] concentrations. As depicted in Fig. 2, the contact value of MEP at first OHP continuously decreases as the concentration of divalent ion increases. The faster decay of MEP near the interface is accompanied by an increase in the same a little away from the interface, indicating a change in sign. There is an increase in the depth of the inversion, although, the width of the inversion layer remains more or less constant. The density and the MEP profiles predicted by the present DFT are in quantitative agreement with the MC data over the entire range of concentrations as seen with the variations in [Mg^{2+}]:[Na^+].

Interesting situation emerges as the charge on the macroion turns negative. Fig. 3 depicts the density profiles of counterions (Na^+ and Mg^{2+}) and coions (Cl^-) as the ratio of [Mg^{2+}]:[Na^+] increases around a macroion of $R = 1.5$ nm with $Q = -0.102$ Cm^{-2} ($Z_M = -18$). The substantial increase in coion concentration in the second OHP lead to considerable OC phenomena as more and more divalent counterion is added. With small amount of divalent salt ($MgCl_2$), [Fig. 3(a)], the contact density of Mg^{2+} at the macroion surface is increased substantially accompanied by the substantial decrease of Na^+. This is quite obvious because of higher valency of Mg^{2+} as compared to Na^+. However, with more

Mg^{2+} is added, the contact density started decreasing because of screening of the surface charge on the macroion. The is also reflected with the increase in CR effect with Mg^{2+}, which shifted to a shorter distance. This is quite evident from the MEP profiles, where the contact density at IHP continuously increases with increase in $[Mg^{2+}]$:$[Na^{+}]$ ratio. In effect, size correlations due to volume exclusion has also become equally important like charge correlations in this system. Once again the theoretical prediction and MC data go hand in hand.

The effect of bulk ion-ion correlations of small ions is studied by increasing the bulk concentration of NaCl from 0.01 M to 2M, while maintaining the $[Mg^{2+}]$:$[Na^{+}]$ = 1:2. As can be seen in Fig. 5, the volume exclusion becomes extremely important leading to increase in oscillations in all the ionic density profiles. The double layer becomes more compact and the diffuse layer is narrowed down due to increase in ion-ion correlations. This lead to an effective screening of macroion charge resulting into CR effect as is depicted in Fig. 6. The CR is observed twice because of synergy in size and charge correlation. The "periodicity" of oscillations in the density profiles relates to the diameter of the individual ionic components. The layering and the charge inversion becomes quite distinct, although these are originating from the same physical phenomena. There is substantial increase in the depth of the inversion layer, however, its width decreases due to stronger electrostatic interactions. Quite surprisingly, the DFT predictions show quantitative matching with MC simulation. This is in sharp contrast to our earlier works on size-asymmetric electrolytes.[43]

To study the implications due to variation in the surface charge density on SDL, formed from 1 M NaCl/$MgCl_2$ with $[Mg^{2+}]$:$[Na^{+}]$=1:2 around a macroion of R = 1.5 nm, Q is continuously varied from 0.102 to 0.408 Cm^{-2} (corresponding variation in total charge on the nanoparticle from Z_M = 18 to Z_M = 72). This is depicted in Fig. 7, where there is considerable accumulation of coumterions and depletion of coions from the interface as Q increases. The stronger electrostatic attraction between the counterion and the macroion also lead to effective screening of the macroion charge resulting into charge inversion. Once the inversion sets in, the width as well as the depth of the double layer remains constant. The same conclusions can be drawn from the MEP profiles as shown in Fig. 8.

The charge correlations in SDL is better understood in terms of the size of the macroion alongwith its surface charge density. This is shown in Fig. 9 for a 1 M NaCl/$MgCl_2$ mixed electrolyte with $[Mg^{2+}]$:$[Na^{+}]$=1:2 at Q=0.102 Cm^{-2} for four different macroion radii, viz.

$R = 0.5$ nm, 1 nm, 1.5 nm, and 6 nm. The total charge on the maacroion for these four sizes corresponds to $Z_M = 2$, 8, 18, and 288 respectively. As we move on to the larger macroion, there is an increase in absolute charge (Z_M) on the macroion resulting into an enhancement of counterions and consequent depletion of coions at the macroion surface. The diffuse layer widens with faster decay of counterions accompanied with sharp growth of coion density profiles at a distance away from the surface. This also results in the increase in CR effect. As evident from the MEP profile in Fig. 10, the depth of CR layer increases, whereas the width remains more or less constant. Once again, the agreement between the theory and simulation results is excellent.

In order to study the effect of valence on the behavior of diffuse layer, the added electrolyte is changed to $AlCl_3$ instead of $MgCl_2$. Thus, Fig. 11 depicts the ionic density and the MEP profiles of NaCl/$AlCl_3$ mixed electrolyte with $[Al^{3+}]$:$[Na^+]$=1:2 with 1 M NaCl. The coion and counterion densities remain almost the same, although there is a slight increase in Cl^- and Al^{3+} at the interface [cf. Fig. 1(c)]. This also resulted in stronger charge inversion for higher valent coion (Al^{3+}) because of excess of counterions effectively screening the surface charge. This is also clear from the MEP profile, where the inversion width essentially gets reduced (cf. Fig. 2).

The importance of size correlations is also envisaged with change in ionic sizes (σ) of the small ions. Fig. 12 shows the ionic density profiles for 1 M NaCl with added $MgCl_2$ for $[Mg^{2+}]$:$[Na^+]$=1:2 at four different smallest ionic diameters, viz. $\sigma = 0.1$ nm, 0.15 nm, 0.2 nm, and 0.25 nm. For smallest $\sigma = 0.1$ nm, the counterion (Cl^-) density profile decays monotonically at the expense of growth of coion (Na^+ and Mg^{2+}) density profiles. However, the diffuse layer gets compacted for $\sigma = 0.15$ nm because of stronger size correlations. As the ionic size is increased to $\sigma = 0.2$ nm, the size correlation converts to charge correlation leading to charge inversion at a distance away from the interface. At the largest ionic sizes studied here for $\sigma = 0.25$ nm, the double layer become more structured with the presence of another layers for counterions (Cl^-) and monovalent coions (Na^+). This is due to the volume exclusion resulted from the larger ionic sizes. In fact, this system alongwith the concentration variation (cf. Fig.5) show clear evidence of distinctive contribution from size and charge correlations. This step by step effect of correlations can also be visualized in the MEP profiles shown in Fig. 13, which also indicates double charge inversions for the case of largest ionic size ($\sigma = 0.25$ nm). The increase of the amount of coions at all the Helmholtz

planes is an indication of increase of OC effect with increase in small ionic sizes. The double layer also becomes thinner and deeper as is evident from both the density as well as MEP profiles. The DFT predictions are in quantitative agreement with MC profiles for all the ionic diameters studied in the present work.

IV. CONCLUDING REMARKS

A systematic study on the effect of multivalent ions on the structure of spherical electric double layers is studied here with the gradual addition of multivalent ion in a normal monovalent PM electrolyte solution. The sizes of all the three components of the PM electrolyte are distinct to have individual influence on the static properties of the SDL formed. A critical comparison has been attempted here using density functional theory and Monte Carlo simulations. A partially perturbative approach involving weighted density approximation is used for DFT study. The direct correlation functions for the bulk electrolyte required for the present DFT are from the MSA solution of n component bulk electrolyte of arbitrary charge and size asymmetry due to Blum[55] and Heroike.[56] The system is studied under variation of several parametric conditions, viz. the concentration ratios of mono- and multivalent ions, the bulk concentration of the mixed electrolytes, size of macroion and surface charge densities as well as size of small ions. The excellent agreement between the theoretical predictions and the Monte Carlo data over the wide range of parametric conditions indicates the suitability of the present DFT. Comparison to the binary PM electrolyte vis a vis to that of RPM system is presented in a number of situations.

The importance of OC and CR effects are clearly reflected with the addition of multivalent ions in PM electrolytes. The present work provides direct support of the important fact that coions becomes extremely important in SDL formed from PM electrolyte unlike RPM, where counteions determine the very nature of SDL formed. The interplay between charge and size correlations have important implications on the diffuse layer characteristics in terms of compactness as well as in charge inversions. Thus ionic correlations became important with increase in $[Mg^{2+}]$:$[Na^{+}]$ ratio, bulk concentrations, size of macroion, and surface charge density on the macroion. Similarly, the size correlation takes precedence with increase in the size of the small ions of the mixed electrolytes. such as charge inversions and zeta potentials. Thus, The addition of divalent coions (Mg^{2+}) to the 1:1 (NaCl) electrolyte system causes

the decrease of layering of counterions (Cl^-). The formation of multiple layers at large bulk concentration and in the case of largest small ion is indicative of the distinctive contribution of the charge and size correlations in SDL formed from PM electrolyte solution. The effective screening of macroion surface charge also lead to important conclusions regarding depth and width of inversion layers.

The present primitive model used to study the mixed electrolyte system is a completely idealized situation, since at these sizes, the non-electrostatic effect such as ionic polarizability will have sufficient contributions.[59] The interaction between hydration shells around individual nanoparticles as well as that of other nanoparticles is also important. The actual atomistic structure of the nanoparticle itself will be another factor determining the SDL formed. A detailed insight in such situations may emerge from the use of more civilized models[60] as well as explicit interactions from the solvent and ions.[61]

The present work can be equally important in cylindrical geometry as that will provide important information concerning DNA conformation in different supporting electrolyte solutions,[62] which gives a direct mechanism to control the gene expression. The addition of solvent and its associated effects are another important area that requires immediate attention.[63] The other work should be to predict the electrokinetic charge of the colloidal macroion in electrophoresis since this is related to MEP at the slipping plane.[64] The present theory can be directly applicable to calculate the force between the large colloidal particles immersed in a mixed electrolyte solution and provide important implications about the nature of forces involved.[65] At present, work along these directions are in progress and will be reported in future.

Acknowledgments

The author gratefully acknowledges Swapan K. Ghosh for helpful discussions during this work. It is a pleasure to thank B.N. Jagatap for his kind interest and constant encouragement.

---

* Also at Homi Bhabha National Institute, Mumbai, India; Electronic mail: chandra@barc.gov.in

[1] J. Ramsden, *Applied Nanotechnology* (Elsevier, UK, 2009).

[2] M. Stepanova and S. Dew, *Nanofabrication* (Springer, Wien, New York, 2012).

[3] *Molecules at Work*, edited by B. Pignataro (Wiley-VCH, Weinheim, 2012).

[4] J.I Park, T.D. Nguyen, G. de Queirós Silveira, J.H. Bahng, S. Srivastava, G. Zhao, K. Sun, P. Zhang, S.C. Glotzer and N.A. Kotov, Nature Communications **5** 3593, (2014)

[5] S.H. Chung, B.J. Choi, S. W. Lee, and D.S. Yoon, Biomedical Engineering Letters, **1**, 7 (2011).

[6] S. Datta, *Lessons from Nanoelectronics* (World Scientific, Singapore, 2012).

[7] *Advances in Macromolecules*, edited by M.V. Russo (Springer, Netherlands, 2010).

[8] K. Azuma, S. Ifuku, T. Osaki, Y. Okamoto, Y and S. Minami, J. Biomed. Nanotechnol. **10**, 2891 (2014).

[9] M.A. Taylor, J. Janousek, V. Daria, J. Knittel, B. Hage, H. Bachor, and W.P. Bowen, Nature Photon. **7**, 229 (2013).

[10] A. Ashkin and J.M. Dziedzic, Science **235** 1517 (1987).

[11] A Boyde, Science **230**, 1270 (1985).

[12] Carnie, S.L.; Torrie, G.M. *Adv. Chem. Phys.* **1984**, *56*, 141.

[13] P. Attard, Adv. Chem. Phys. **92**, 1 (1996).

[14] Schmitz, K. S. *Macroions in Solution and Colloidal Suspension*; VCH: New York, 1993.

[15] Torrie, G.M.; Valleau, J.P. *J. Chem. Phys.* **1980**, *73*, 5807; *J. Phys. Chem.* **1982**, *86*, 3251.

[16] Mills, P. ; Anderson, C.F.; Record, M.T., Jr., *J. Phys. Chem.* **1985**, *89*, 3984.

[17] Tanford, C. *Physical Chemistry of Macromolecules*; Wiley: New York, 1961.

[18] Outhwaite, C.W.; Bhuiyan, L.B. *Electrochimica Acta* **1991**, *36*, 1747.

[19] L. Blum and D. Henderson, in *Fundamentals of Inhomogeneous Fluids*, edited by D. Henderson (Dekker, New York, 1992).

[20] Evans, R. in *Fundamentals of Inhomogeneous Fluids*; Henderson D., Ed.; Marcel Dekker: New York, 1992.

[21] Lozada-Cassou, M. *J. Chem. Phys.* **1981**, *75*, 1412; *J. Chem. Phys.* **1982**, *77*, 5258.

[22] Outhwaite, C.W.; Bhuiyan, L.B. *J. Chem. Phys.* **1986**, *85*, 4206.

[23] Mier-y-Teran, L.; Diaz-Herrera, E.; Lozada-Cassou, M.; Henderson, D. *J. Phys. Chem.* **1988**, 92, 6408.

[24] Mier-y-Teran, L.; Suh, S.H.; White, H.S.; Davis, H.T. *J. Chem. Phys.* **1990**, *92*, 5087.

[25] C.N. Patra *J. Chem. Phys.* **1990**, *111*, 9832.

[26] Jiang, J.; Cao, D.; Henderson, D.; Wu, J. *Phys. Chem. Chem. Phys.* **2014**, *140*, 044714.

[27] Lozada-Cassou, M. *J. Phys. Chem.* **1983**, *87*, 3729.

[28] González-Tovar, E.; Lozada-Cassou, M.; Henderson, D. *J. Chem. Phys.* **1985**, *83*, 361.

[29] Patra, C.N.; Yethiraj, A. *J. Phys. Chem. B* **1999**, **103**, 6080.

[30] Wang, K.; Yu, Y.-X.; Gao, G.-H.; Luo, G.-S. *J. Chem. Phys.* **2005**, *123*,234904.

[31] Grimson, M.J..; Rickayzen, G. *Chem. Phys. Lett.* **1982**, *86*, 71.

[32] H. Greberg and R. Kjellander, J. Chem. Phys. **108**, 2940 (1998).

[33] D. Gillespie, M. Valiskó, and D. Boda, J. Phys.: Condens. Matter **17** 6609 (2014).

[34] Guerrero-García, G.I.; González-Tovar, E.; Lozada-Cassou, M.; Guevara-Rodríguez, F. de J. *J. Chem. Phys.* **2005**, *123*, 034703.

[35] Bhuiyan, L.B.; Outhwaite, C.W. *J. Colloid Interface Sci.* **2009**, *331*, 543.

[36] Guerrero-García, G.I.; González-Tovar, E.; Olvera de la Cruz, M. *J. Chem. Phys.* **2011**,*135*, 054701.

[37] Torrie G.M.; Valleau, J.P.; Patey, G.N. *J. Chem. Phys.* **1982**, *76*, 4615.

[38] Guerrero-García, G.I.; González-Tovar, E.; Chávez-Páez, M. *Phys. Rev. E* **2009**, *80*, 021501.

[39] Guerrero-García, G.I.; González-Tovar, E.; Chávez-Páez, M.; Lozada-Cassou, M. *J. Chem. Phys.* **2010** *132*, 054903.

[40] Guerrero-García, G.I.; González-Tovar, E.; Olvera de la Cruz, M. *Soft Matter* **2010**, *6*, 2056.

[41] Kim, E.-Y.; Kim, S.-C. *J. Chem. Phys.* **2014**, *140*, 154703.

[42] Medasani, B.; Ovanesyan, Z.; Thomas, D.G.; Sushko, M.L.; Marucho, M. *J. Chem. Phys.* **2014**, *140*, 204510.

[43] Patra, C.N. *J. Chem. Phys.* **2014**, *141*, 184702.

[44] Jiménez-Ángeles, F.; Lozada-Cassou, M. *J. Chem. Phys.* **2004**, *108*, 7286.

[45] Gelbart, W.M.; Bruinsma, R.F.; Pincus, P.A.; Parsegian, V.A. *Phys. Today* **2000**, *53*, 38.

[46] C.V. Bizarro1, A. Alemany, and F. Ritort, Nucleic Acids Research, **40**, 6922 (2014).

[47] A. Martín-Molina, M. Quesada-Peŕez, and R. Hidalgo-Álvarez, J. Phys. Chem. B **110**, 1326 (2006).

[48] Patra, C.N. *J. Phys. Chem. B* **2010**, *114*, 10550.

[49] M. Kanduc, A. Naji, J. Forsman and R. Podgornik, J. Chem. Phys. **137**, 174704 (2012).

[50] Z. Wang, Y. Xie, Q. Liang, Z. Ma, and J. Wei, J. Chem. Phys. **137**, 174704 (2012).

[51] T. Goel, C.N. Patra, S.K. Ghosh, and T. Mukherjee J. Chem. Phys. **132**, 194706 (2010).

[52] A.R. Rakitin and G.R. Pack, J. Phys. Chem. B **108**, 2712 (2004).

[53] González-Tovar, E.; Lozada-Cassou, M. *J. Phys. Chem.* **1989**, *93*, 3761.

[54] Denton, A.R.; Ashcroft, N.W. *Phys. Rev. A* **1991**, *44*, 8242.

[55] Blum, L. *Mol. Phys.* **1975**, *30*, 1529.

[56] Hiroike, K. *Mol. Phys.* **1977**, *33*, 1195.

[57] Metropolis, N.; Rosenbluth, A.W.; Rosenbluth, M.N.; Teller, A.H.; Teller, E. *J. Chem. Phys.* **1953**, *21*, 1087.

[58] Frenkel, D.; Smit, B. *Understanding Molecular Simulation*; Academic Press: New York, 2002.

[59] Guerrero-García, G.I.; Olvera de la Cruz, M. *J. Phys. Chem. B* **2014**, *118*, 8854.

[60] Zwanikken, J.W.; Olvera de la Cruz, M. *Proc. Natl. Acad. Sci. USA* **2013**, *110*, 5301.

[61] Mittal, J.; Best, R.B. *Proc. Natl. Acad. Sci. USA* **2008**, *105*, 20233.

[62] S. Gavryushov, J. Phys. Chem. B **113**, 2160 (2009).

[63] P. Mentré, J. Biol. Phys. **38**, 13 (2012).

[64] E. Sánchez-Arellanoa, W. Olivares, M. Lozada-Cassou, and F. Jiménez-Ángeles, J. Colloid Interface Sci. **330**, 474 (2009).

[65] O. Trotsenko, Langmuir **230**, 6037 (2012).

Figures

FIG. 1: Ionic density profiles around a spherical macroion of $R = 1.5$ nm and $Q = 0.102$ Cm^{-2} having 1 M NaCl with added $MgCl_2$ with different $[Mg^{2+}]$:$[Na^+]$ concentration ratio as: (a) pure NaCl, (b) 1:4, (c) 1:2, and (d) pure $MgCl_2$. Symbols are simulation results and lines represent the present DFT. Na^+: (Black, □), Cl^-: (Green, ○), and Mg^{2+}: (Red, △).

FIG. 2: Mean electrostatic potential profiles around a spherical macroion of $R = 1.5$ nm and $Q = 0.102$ Cm^{-2} having 1 M NaCl with added $MgCl_2$ with different $[Mg^{2+}]$:$[Na^+]$ concentration ratio as: 1:16 (Black, □), 1:8 (Green, ○), 1:4 (Blue, △), and 1:2 (Red, ⋆). Symbols are simulation results and lines represent the present DFT.

FIG. 3: Ionic density profiles around a spherical macroion of $R = 1.5$ nm and $Q = -0.102$ Cm^{-2} having 1 M NaCl with added $MgCl_2$ with different $[Mg^{2+}]$:$[Na^+]$ concentration ratio as: (a) pure NaCl, (b) 1:4, (c) 1:2, and (d) pure $MgCl_2$. Symbols are simulation results and lines represent the present DFT. Na^+: (Black, □), Cl^-: (Green, ○), and Mg^{2+}: (Red, △).

FIG. 4: Mean electrostatic potential profiles around a spherical macroion of $R = 1.5$ nm and $Q = -0.102$ Cm^{-2} having 1 M NaCl with added $MgCl_2$ with different $[Mg^{2+}]$:$[Na^+]$ concentration ratio as: 1:16 (Black, □), 1:8 (Green, ○), 1:4 (Blue,△), and 1:2 (Red, ⋆). Symbols are simulation results and lines represent the present DFT.

FIG. 5: Ionic density profiles around a spherical macroion of $R = 1.5$ nm and $Q = 0.102$ Cm^{-2} for $NaCl/MgCl_2$ salt with $[Mg^{2+}]$:$[Na^+]$ = 1:2, at various concentrations as: (a) 0.01 M, (b) 0.1 M, (c) 1 M, and (d) 2 M. The key is the same as in Fig. 1.

FIG. 6: Mean electrostatic potential profiles around a spherical macroion of $R = 1.5$ nm and $Q = 0.102$ Cm^{-2} for NaCl/$MgCl_2$ salt with $[Mg^{2+}]$:$[Na^+] = 1$:2, at various concentrations as: 0.01 M (Green, ○), 0.1 M (Blue, △), 1 M (Red, ⋆), and 2 M (Black, □). Symbols are simulation results and lines represent the present DFT.

FIG. 7: Ionic density profiles for 1 M NaCl/$MgCl_2$ salt with $[Mg^{2+}][Na^+] = 1$:2, around a spherical macroion of $R = 1.5$ nm at varying surface charge densities: (a) $Q = 0.102$ C/m^2, (b) $Q = 0.204$ C/m^2, (c) $Q = 0.306$ C/m^2, and (d) $Q = 0.408$ C/m^2. The key is the same as in Fig. 1.

FIG. 8: Mean electrostatic potential profiles for 1 M NaCl/$MgCl_2$ salt with $[Mg^{2+}][Na^+] = 1$:2, around a spherical macroion of $R = 1.5$ nm at varying surface charge densities: $Q = 0.102$ C/m^2 (Black, □), $Q = 0.204$ C/m^2, (Red, ⋆), $Q = 0.306$ C/m^2 (Blue, △), and $Q = 0.408$ C/m^2 (Green, ○).

FIG. 9: Ionic density profiles for 1 M NaCl/$MgCl_2$ salt with $[Mg^{2+}][Na^+] = 1$:2, around a spherical macroion of $Q = 0.102$ Cm^{-2} at different macroion radii: (a) $R = 0.5$ nm, (b) $R = 1$ nm, (c) $R = 1.5$ nm, and (d) $R = 6$ nm. The key is the same as in Fig. 1.

FIG. 10: Ionic density profiles for 1 M NaCl/$MgCl_2$ salt with $[Mg^{2+}][Na^+] = 1$:2, around a spherical macroion of $Q = 0.102$ Cm^{-2} at different macroion radii: $R = 0.5$ nm (Black, □), $R = 1$ nm (Red, ⋆), $R = 1.5$ nm (Blue, △), and $R = 6$ nm (Green, ○).

FIG. 11: Ionic density (a) and mean electrostatic potential (b) profiles for 1 M NaCl/$AlCl_3$ salt with $[Al^{3+}][Na^+] = 1$:2, around a spherical macroion of $R = 1.5$ nm and $Q = 0.102$ Cm^{-2}. Symbols are simulation results and lines represent present DFT. For density profiles (a), Na^+: (Black, □), Cl^-: (Green, ○), and Al^{3+}: (Red, △)

FIG. 12: Ionic density profiles for 1 M NaCl/$MgCl_2$ salt with $[Mg^{2+}][Na^+] = 1$:2, around a spherical macroion of $R = 1.5$ nm and $Q = 0.102$ Cm^{-2} with small ion diameters as (a) $\sigma = 0.1$ nm, (b) $\sigma = 0.15$ nm, (c) $\sigma = 0.2$ nm, and (d) $\sigma = 0.25$ nm . The key is the same as in Fig. 1.

FIG. 13: Mean electrostatic potential profiles for 1 M NaCl/$MgCl_2$ salt with $[Mg^{2+}][Na^{+}] = 1{:}2$, around a spherical macroion of $R = 1.5$ nm and $Q = 0.102$ Cm^{-2} with small ion diameters as $\sigma = 0.1$ nm (Green, $\bigcirc$), $\sigma = 0.15$ nm (Blue, $\triangle$), $\sigma = 0.2$ nm (Red, $\star$), and $\sigma = 0.255$ nm (Black, $\square$).

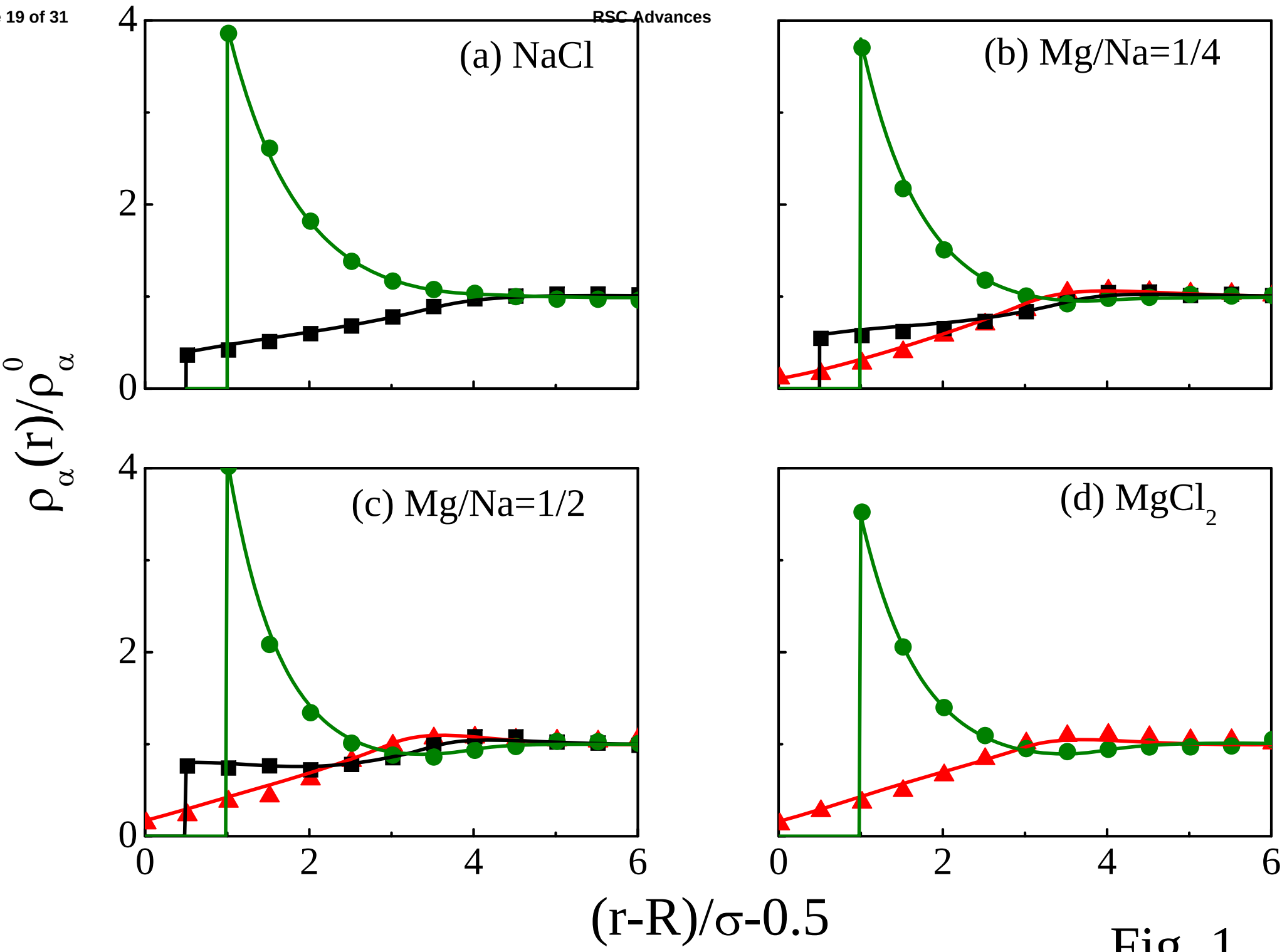

Fig. 1

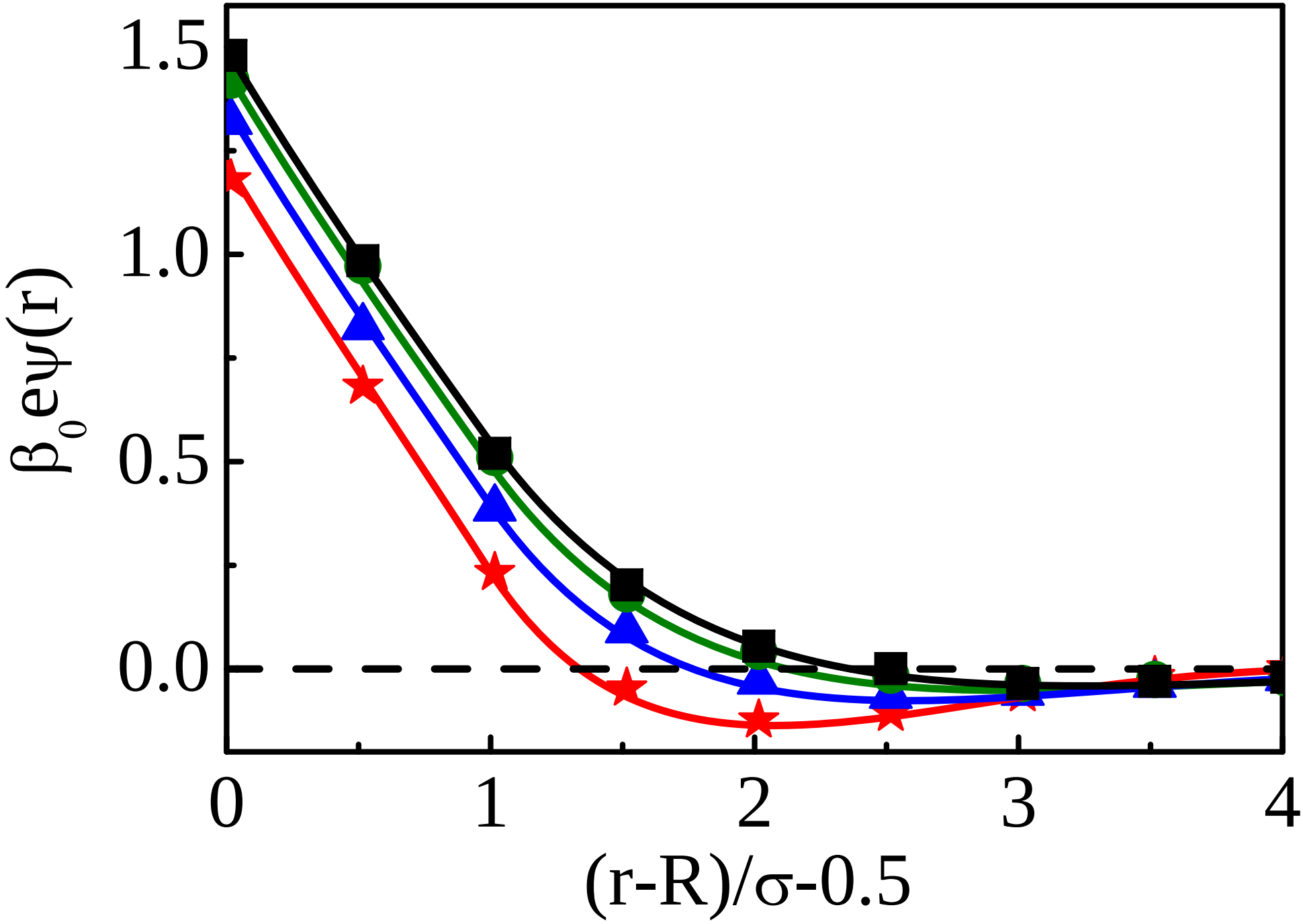

Fig. 2

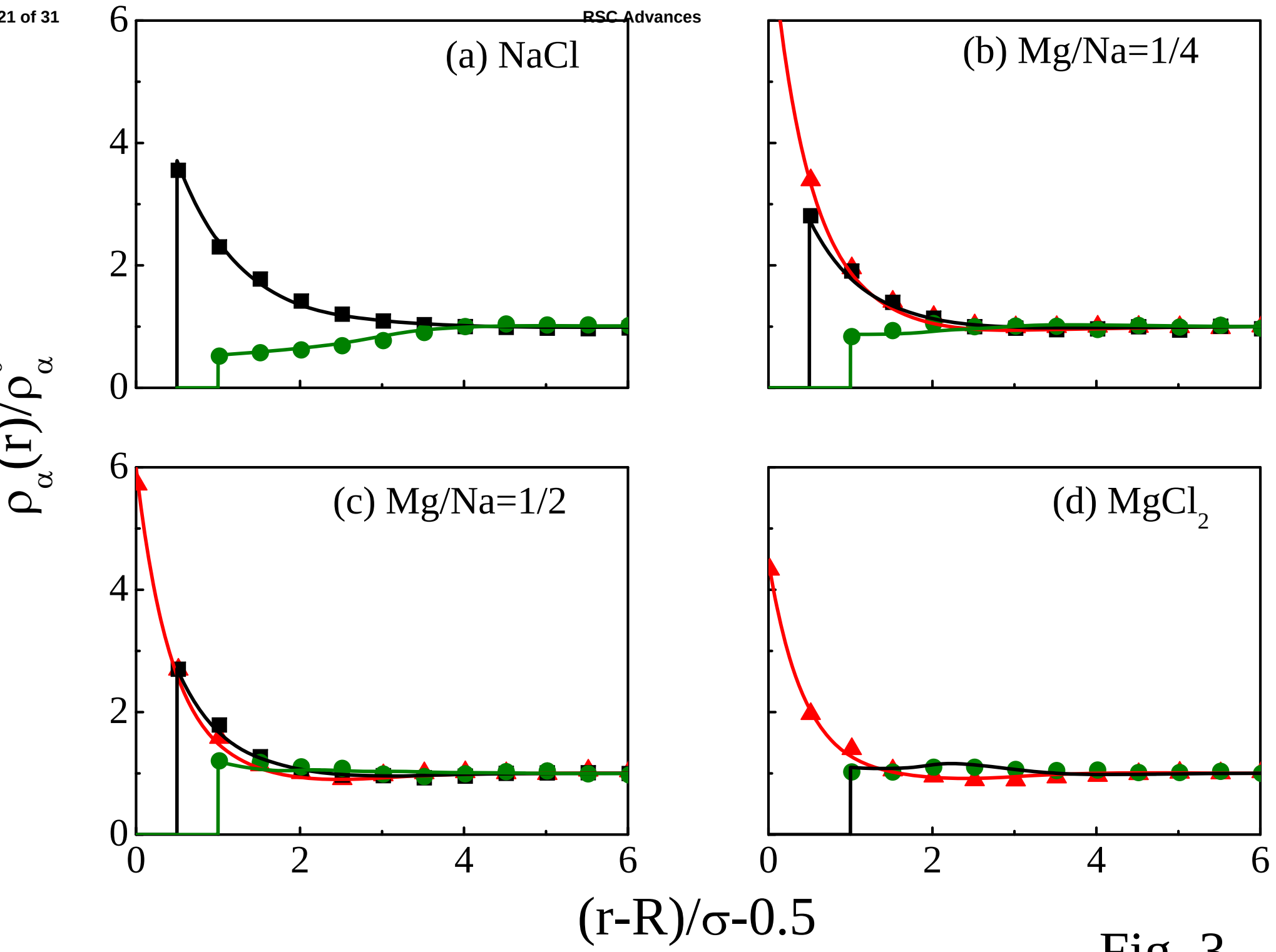

Fig. 3

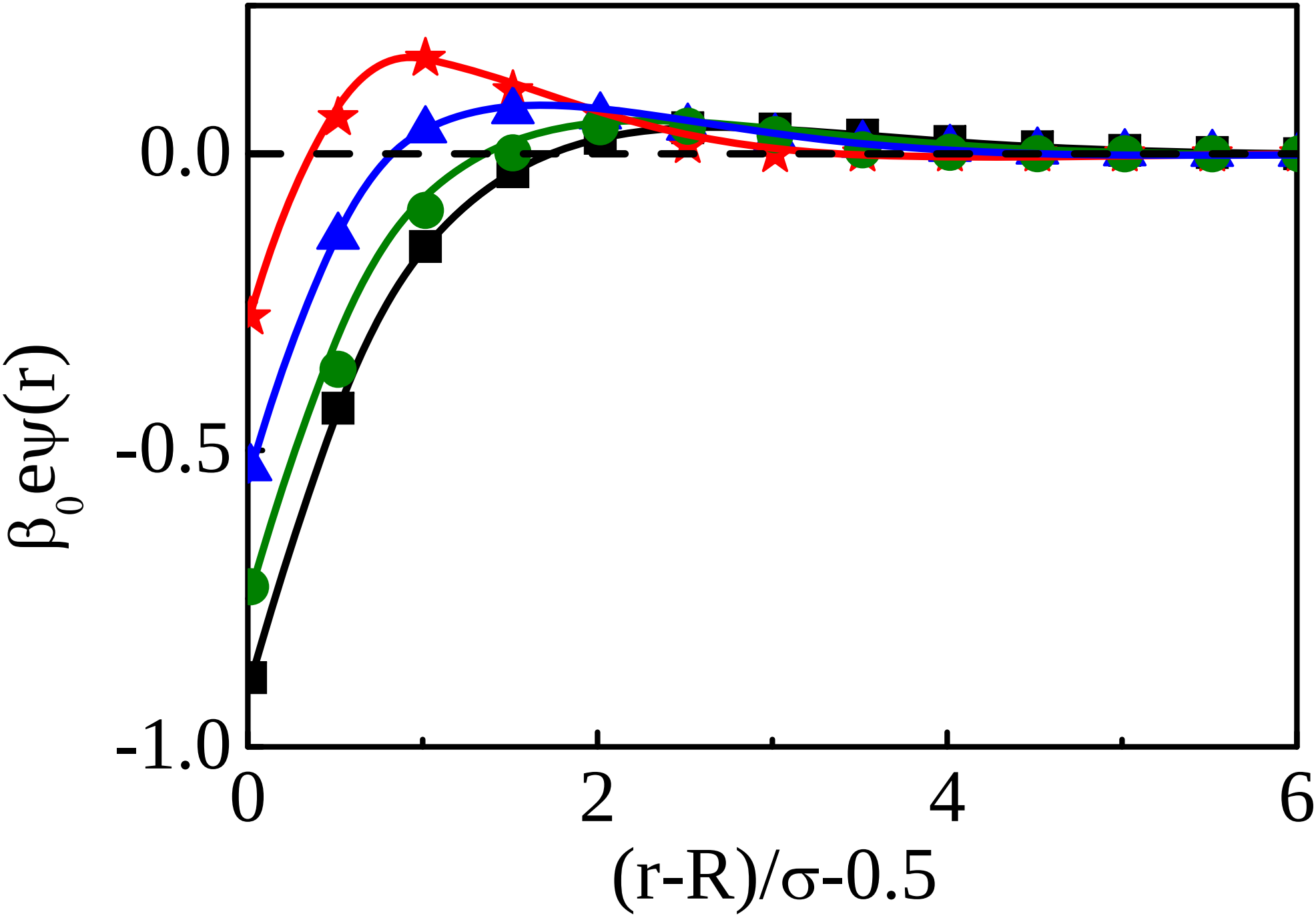

Fig. 4

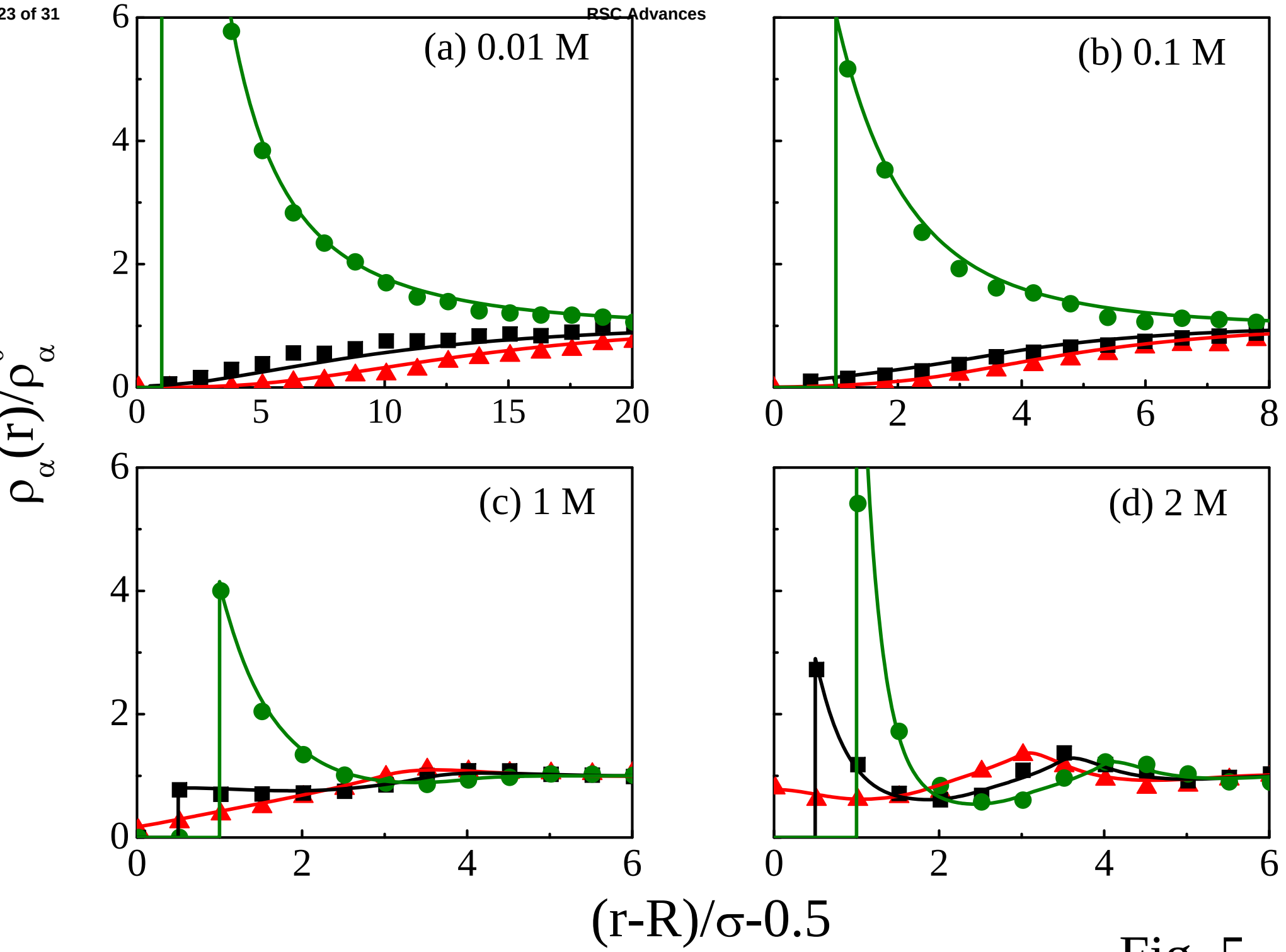

Fig. 5

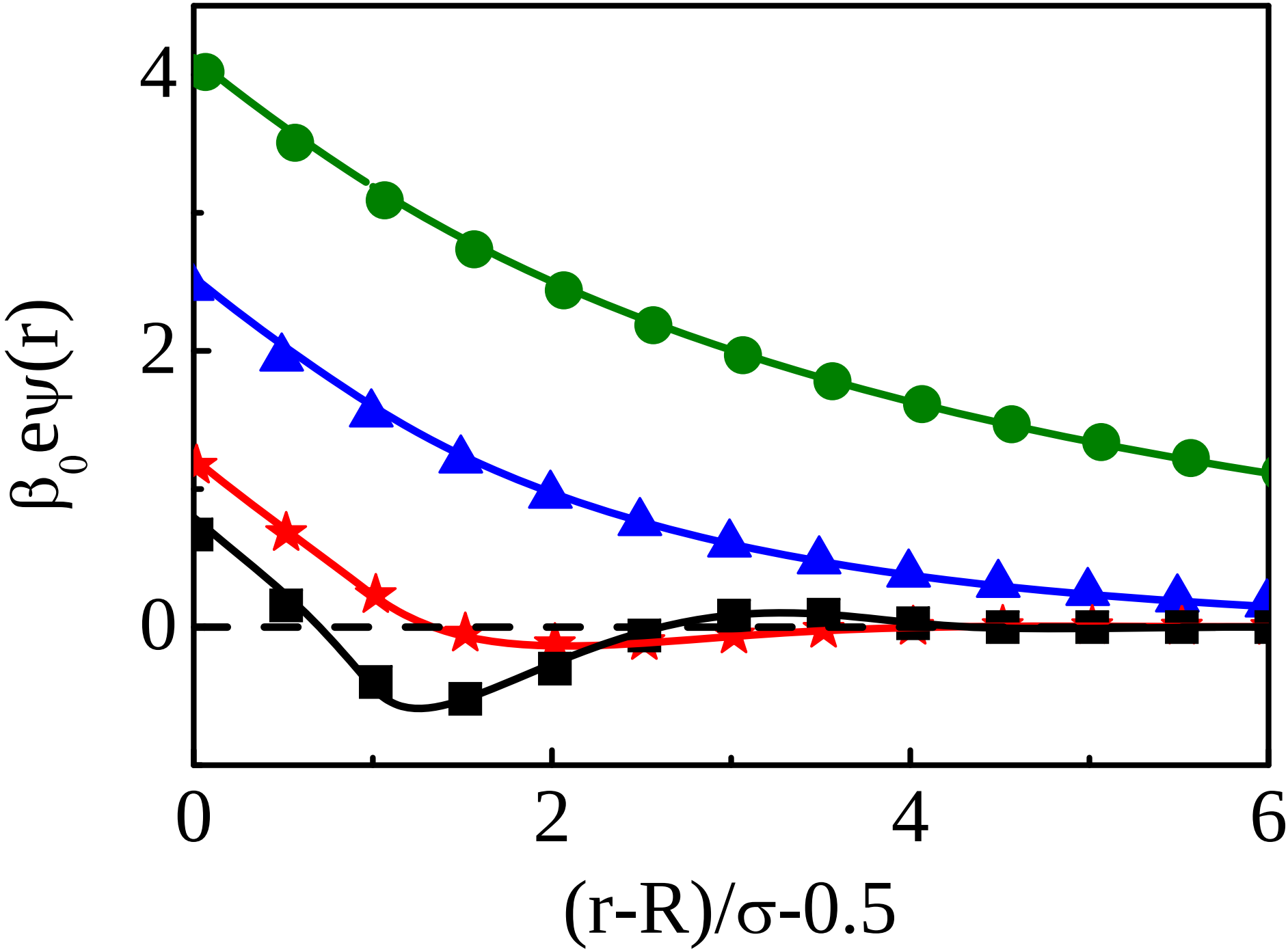

Fig. 6

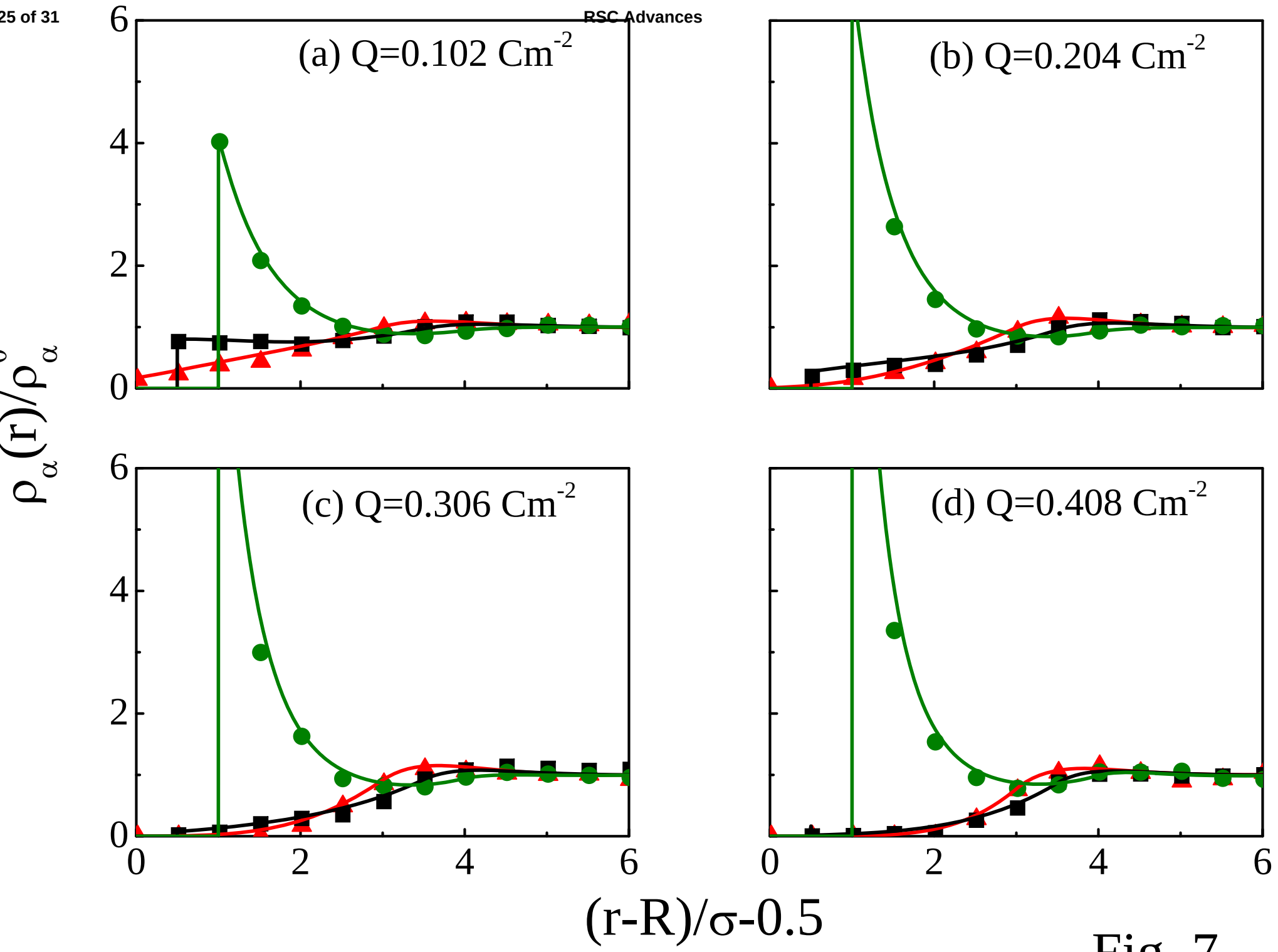

Fig. 7

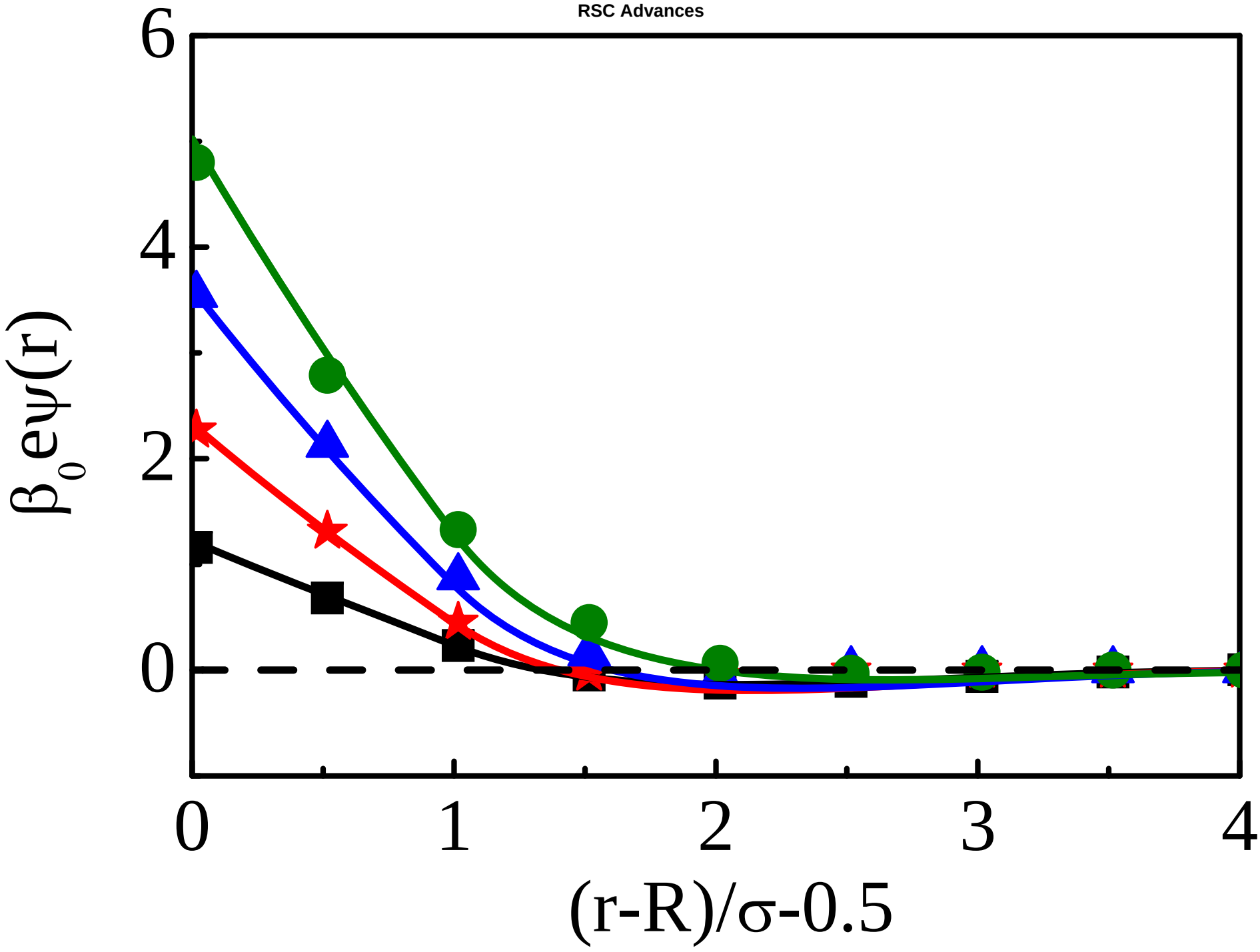

Fig. 8

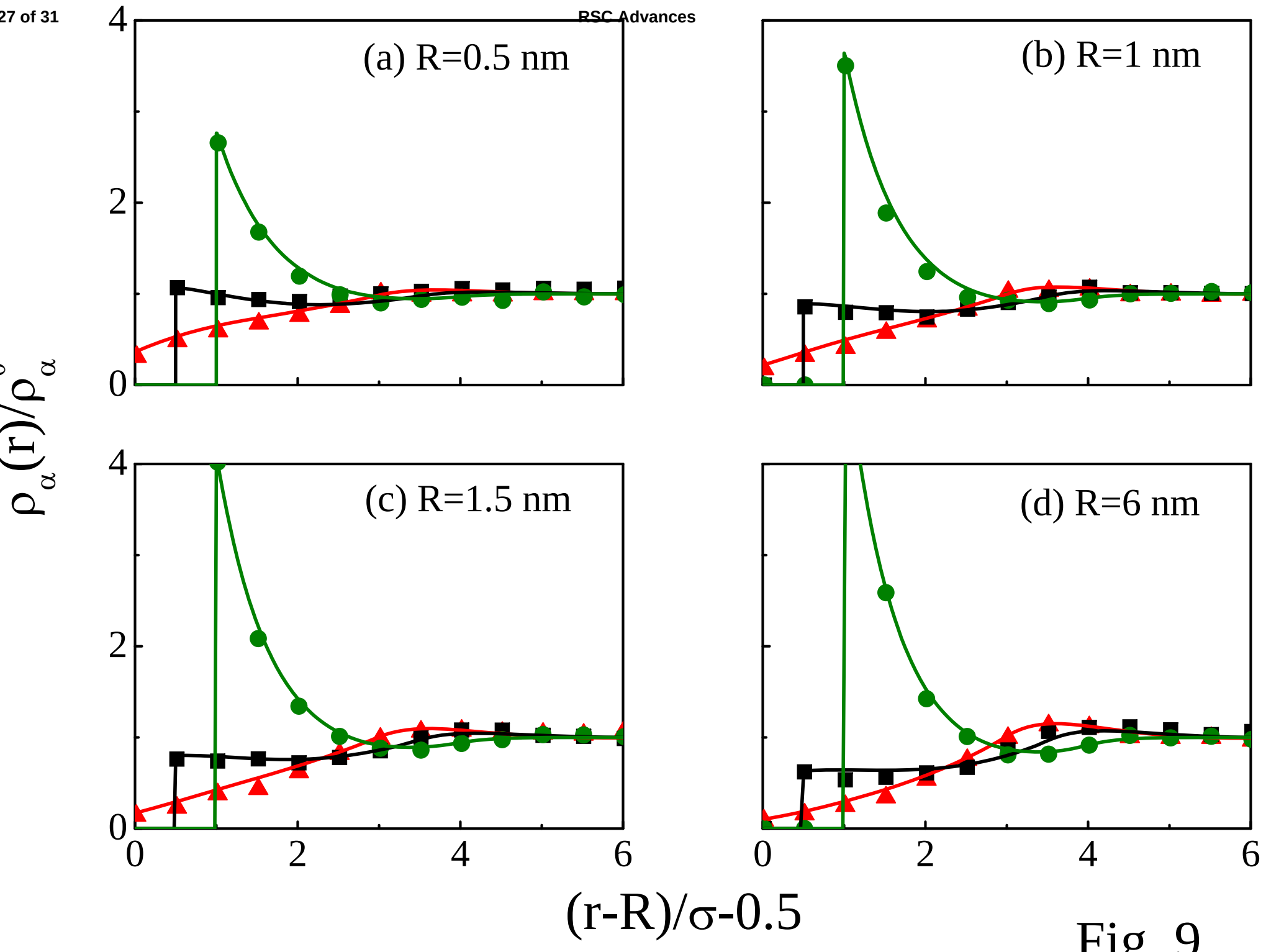

Fig. 9

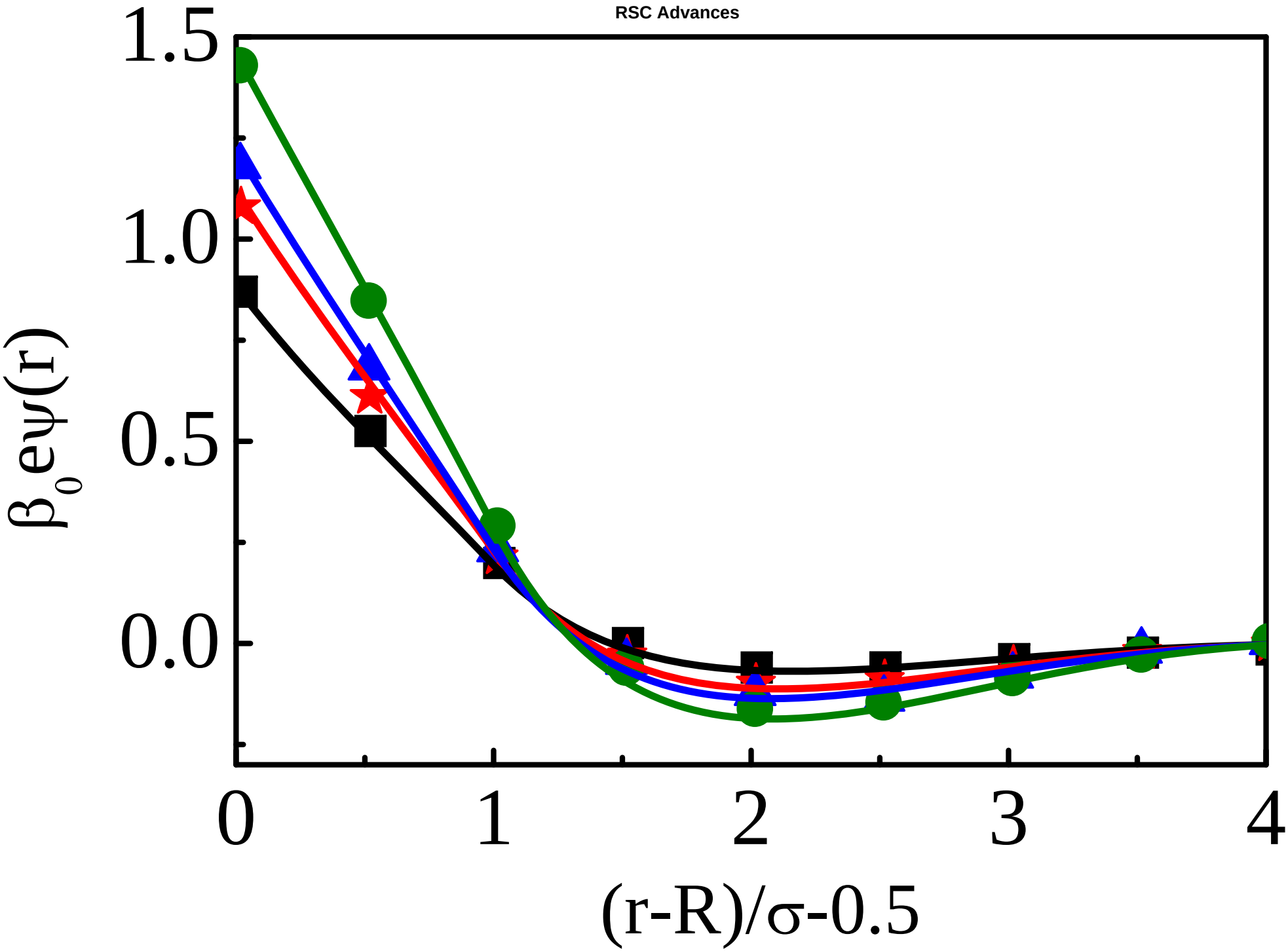

Fig. 10

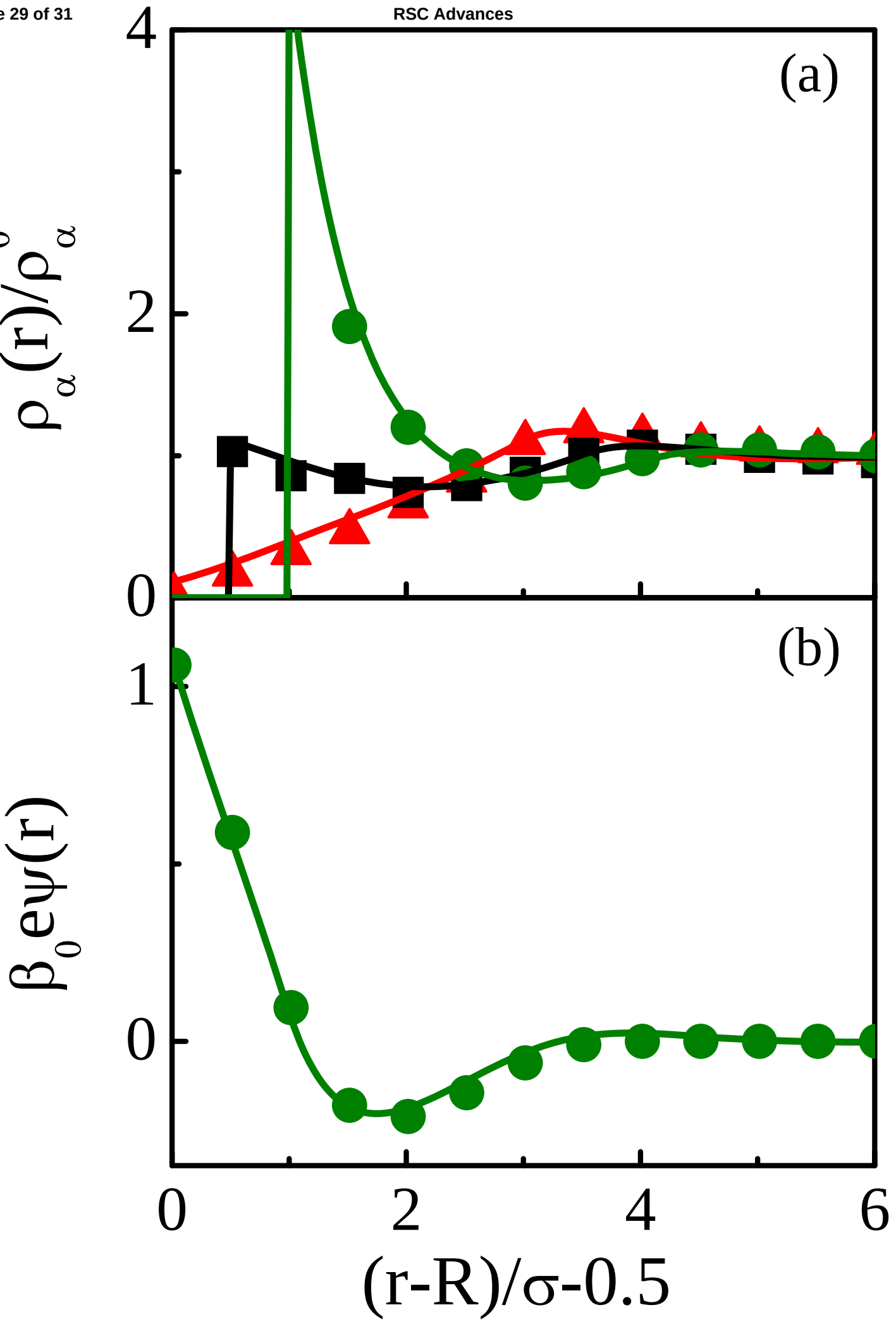

Fig. 11

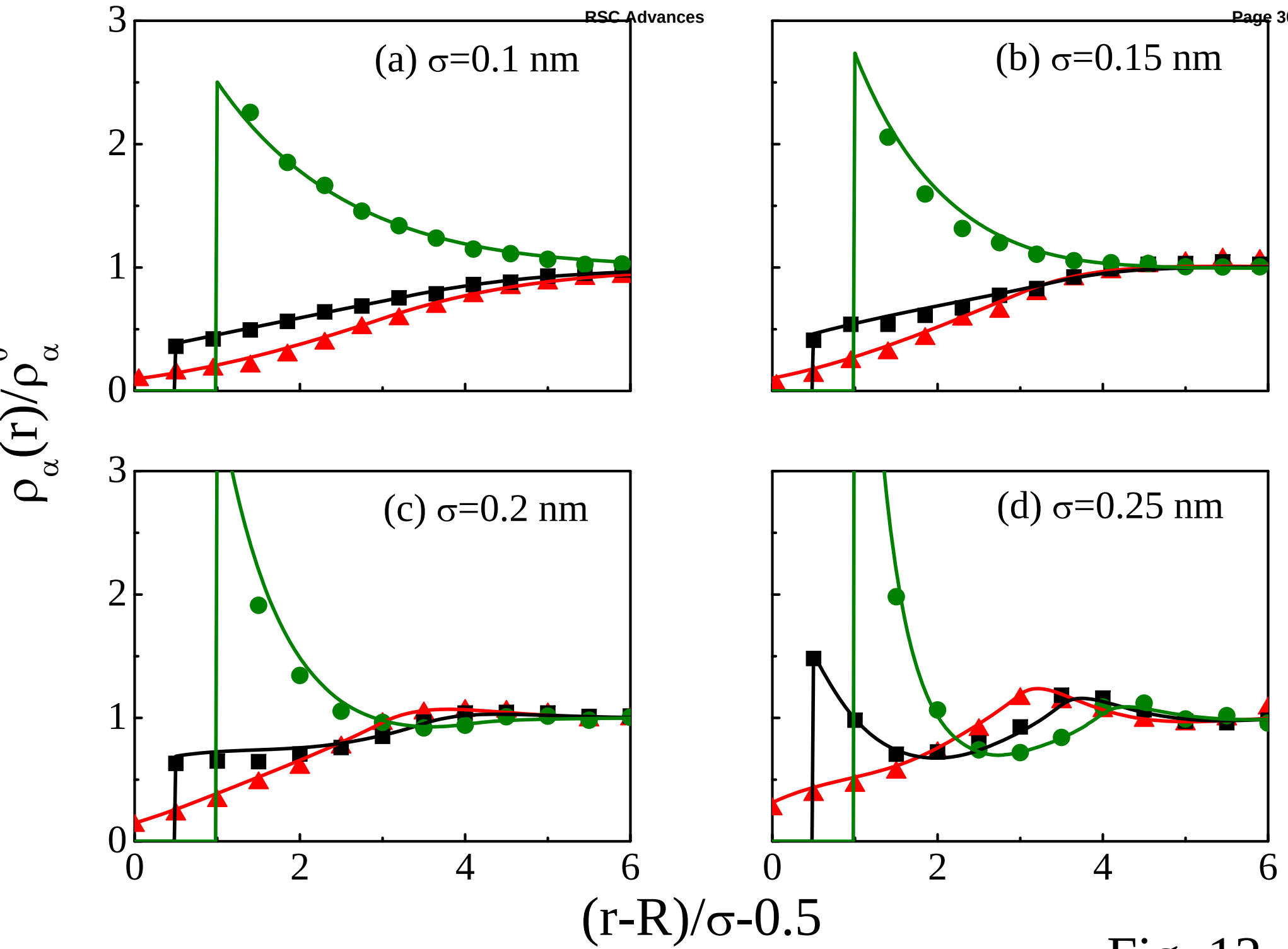

Fig. 12

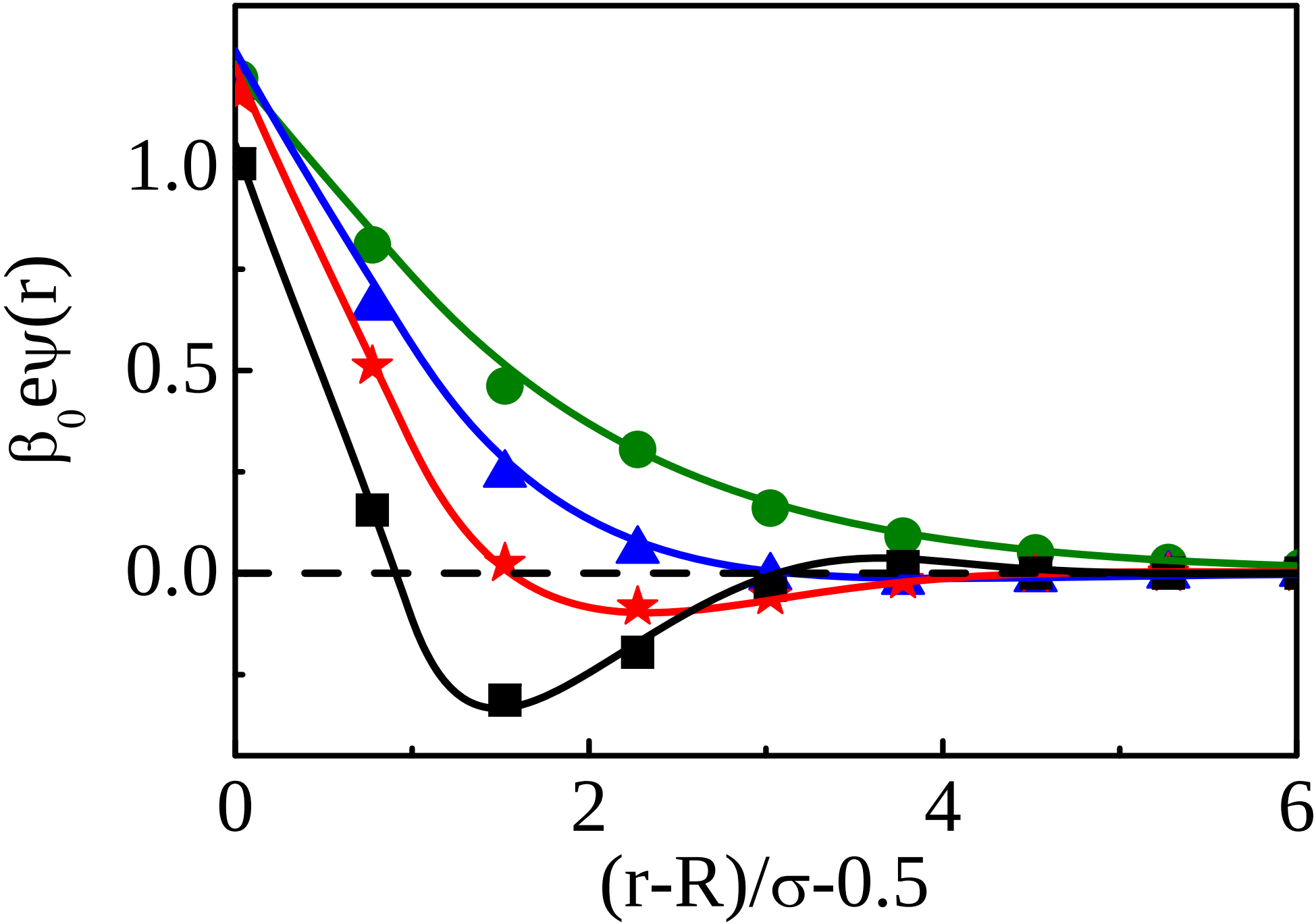

Fig. 13